

# High-Resolution SPECT Imaging of Stimuli-Responsive Soft Microrobots

Veronica Iacovacci,\* Alain Blanc, Henwei Huang, Leonardo Ricotti, Roger Schibli, Arianna Menciassi, Martin Behe, Salvador Pané,\* and Bradley J. Nelson

**Untethered small-scale robots have great potential for biomedical applications. However, critical barriers to effective translation of these miniaturized machines into clinical practice exist. High resolution tracking and imaging in vivo is one of the barriers that limit the use of micro- and nanorobots in clinical applications. Here, the inclusion of radioactive compounds in soft thermoresponsive magnetic microrobots is investigated to enable their single-photon emission computed tomography imaging. Four microrobotic platforms differing in hydrogel structure and four  $^{99m}\text{Tc}[\text{Tc}]$ -based radioactive compounds are investigated in order to achieve optimal contrast agent retention and optimal imaging. Single microrobot imaging of structures as low as 100  $\mu\text{m}$  in diameter, as well as tracking of shape switching from tubular to planar configurations by inclusion of  $^{99m}\text{Tc}[\text{Tc}]$  colloid in the hydrogel structure, is reported.**

Wireless micro- and nanoscale robots are miniaturized structures with the ability to perform tasks under the application of external power sources,<sup>[1]</sup> or by harvesting reagents available in their surroundings.<sup>[2,3]</sup> One of the ultimate goals of these devices is to perform biomedical tasks such as microsurgery or targeted drug delivery in confined locations of the human body.<sup>[4–6]</sup> The issues of locomotion in biologically relevant fluids<sup>[7]</sup> and the release of therapeutic payloads<sup>[8–10]</sup> are currently in focus. Preliminary work with animal models has recently shown the potential of small-scale robots in the biomedical

field.<sup>[11–13]</sup> While much progress has been made during the last decade, several key issues remain unsolved, and work on the development of biocompatible (either biodegradable<sup>[14,15]</sup> or retrievable<sup>[16]</sup>) and “visible” microrobots<sup>[17]</sup> is still required. One of the most challenging issues that prevents the translation of small-scale machines to the clinic is the lack of strategies for the effective tracking and imaging of these devices during their journey in the human body.<sup>[18,19]</sup> A synergistic development of diverse research areas including chemical functionalization of the surface of micro- and nanostructures with contrast agents and advanced imaging technologies is key for further development of untethered small-scale robots for in vivo


application. Advancements in microrobot imaging have been recorded. Nelson and co-workers have shown that a swarm of magnetic helical micromachines functionalized with dyes could be tracked in vivo in the peritoneal cavity of a mouse using near infra-red (NIR) imaging, while simultaneously maneuvering them using rotating magnetic fields.<sup>[20]</sup> Recently, Sanchez and co-workers have succeeded in monitoring populations of catalytic micromotors by positron emission tomography.<sup>[21]</sup> The tracking of magnetic microrobots moving through the abdominal aorta of a mini-pig using X-rays has been demonstrated by Park and co-workers.<sup>[22]</sup> Misra and co-workers capitalized on ultrasound to follow the position of self-propelled microparticles.<sup>[23]</sup> Martel and co-workers,<sup>[24]</sup> and more recently, Zhang and co-workers,<sup>[25]</sup> have used magnetic resonance imaging (MRI) to track the position of magnetic microrobots in small animals. However to date, none of these reports have achieved single microrobot imaging with the ability to detect changes in microrobot configuration. Most clinical imaging techniques employed for microrobot monitoring rely on contrasting the magnetic or acoustic properties of the surrounding tissue, making it difficult to determine microstructures in certain parts of the body. This work investigates the inclusion of an imaging agent, which can guarantee successful imaging independent of the properties of the surrounding tissue.

In addition to localization and imaging problems, microrobot structural materials must be carefully considered for their biocompatibility, retrieval potential, or degradation properties. A current trend in small-scale robotics is the replacement of hard components with soft-bodied building blocks. The use of soft materials in these devices brings several advantages, such

Dr. V. Iacovacci, Dr. H. Huang, Dr. S. Pané, Prof. B. J. Nelson  
Institute of Robotics and Intelligent Systems  
ETH Zurich  
Zurich CH-8092, Switzerland  
E-mail: veronica.iacovacci@santannapisa.it; vidalp@ethz.ch

Dr. V. Iacovacci, Prof. L. Ricotti, Prof. A. Menciassi  
The BioRobotics Institute  
Scuola Superiore Sant'Anna  
Pisa 50126, Italy

A. Blanc, Prof. R. Schibli, Dr. M. Behe  
Center for Radiopharmaceutical Sciences  
Paul Scherrer Institut  
Villigen CH-5232, Switzerland  
Prof. R. Schibli  
Department of Chemistry and Applied Biosciences  
ETH Zurich  
8093 Zurich, Switzerland

 The ORCID identification number(s) for the author(s) of this article can be found under <https://doi.org/10.1002/sml.201900709>.

DOI: 10.1002/sml.201900709

as a safe interaction with biological environments, more articulated locomotion mechanisms, and in many cases, enhanced biocompatibility and biodegradability. Among the wide selection of soft materials available, hydrogels are promising candidates for building blocks of soft small-scale robots. Hydrogels can react upon external stimuli by changing their morphology, through solubilizing or degrading.<sup>[26]</sup> Their chemistry can also be tailored to interact favorably with cells and tissues.<sup>[27,28]</sup> In addition, the physicochemical constitution of hydrogels allows these materials to host different kinds of compounds in their matrix, ranging from drugs, magnetic nanoparticles, and electrically conductive nanorods, to fluorescent dyes, contrast agents, or radioactive tracers.<sup>[29]</sup> The versatility of hydrogels enables the construction of highly integrated micro- and nanorobotic platforms with multiple functionalities. An interesting family of hydrogels that has recently been developed in microrobotics is thermally responsive magnetic nanocomposites. These gels can be remotely controlled using magnetic fields to reach a target location, or to induce a shape transition. These morphological changes are used to modulate their dynamic behavior<sup>[30]</sup> or to release therapeutic agents.<sup>[31,32]</sup>

This study presents for the first time, a magnetically driven theranostic soft microrobot made of a thermally responsive hydrogel bilayer. The micromachine contains magnetic nanoparticles and a radioactive compound acting as an imaging agent in its hydrogel frame. The magnetic nanoparticles can be used to remotely drive the locomotion and trigger the shape transformation of the micro-device (by activating the thermoresponsive gel), while the imaging agent allows the microrobot to be monitored *in vivo*.

The proposed soft microrobot can also transport drugs to be released on demand (Figures S3 and S4, Supporting Information). A radioactive compound placed in the microrobot body allows the device to be monitored with high spatial resolution using different tomographic imaging techniques. The chassis of the microrobot consists of two layers: (i) a thermoresponsive layer (made of *N*-isopropylacrylamide (NIPAAm), acrylamide (AAM), poly(ethyleneglycol) diacrylate (PEGDA), 2,2-dimethoxy-2 phenylacetophenone, and ethyl lactate (EL)) in which magnetic nanoparticles are embedded, and (ii) a supporting layer (made of PEGDA) doped with <sup>99m</sup>Tc[Tc] to enable single-photon emission computed tomography (SPECT) imaging of the microrobot (Figure 1A). The different swelling

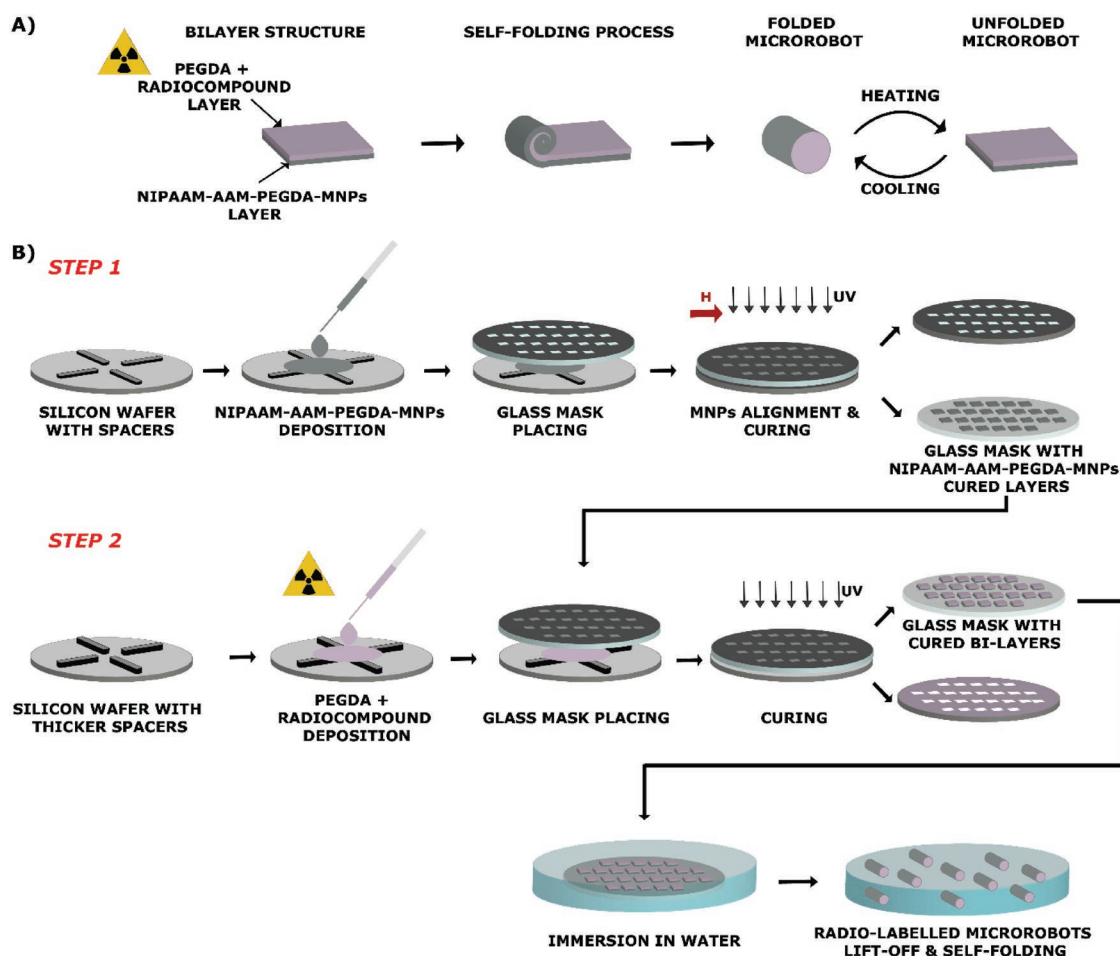


**Figure 1.** Fabrication workflow of shape-switching theranostic soft microrobots. A) Bilayer structure and self-folding mechanism enabling to obtain tubular microrobots able to undergo a shape switching from the folded (tubular) to the unfolded (planar) configuration, due to a change in the thermoresponsive layer swelling state, upon temperature increase. B) Two-steps photolithography fabrication process with inclusion of a radioactive compound in the supporting PEGDA layer.

behavior of the two layers once immersed in water allows the transition from an initial planar configuration to a tubular geometry at body temperature. Shape switching (back to the unfolded planar configuration) can be activated through thermal stimuli (above 42 °C) triggered by NIR stimuli. Microrobots were fabricated according to a previously reported protocol based on two photolithography steps, as illustrated in Figure 1B.

We screened different microrobots of varying dimensions and types of  $^{99m}\text{Tc}[\text{Tc}]$  radioactive compound base. 2D square hydrogel bilayer structures with side lengths of 3, 1.5, and 0.5 mm (thicknesses are reported in Table S1 in the Supporting Information) were successfully produced (Figure S1, Supporting Information). SPECT is a medical imaging technique that is based on conventional nuclear medical imaging and tomographic reconstruction methods. The technique requires the delivery of a gamma-emitting radioisotope (a radionuclide) such as  $^{99m}\text{Tc}$ - or  $^{111}\text{In}$ -based compounds into the patient, normally through injection into the bloodstream. The image device is typically a scintillation camera system which includes a lead collimator and photomultiplier tubes to convert  $\gamma$ ray photons into an electric signal. 3D radioactivity distribution is assessed by combining projection images acquired through 360° rotations of the scintillation camera. In this work, a 4-head multiplexing multi-pinhole camera (NanoSPECT/CTplus, Bioscan Inc., Poway, CA, USA) was used to enable high resolution estimation of 3D radioactivity distribution (Figure 2A). The advantage of SPECT is that the  $\gamma$ rays source is contained within the body and radiation dose is extremely limited when dealing with radio-emitting microrobots. A significant decrease in the absorbed radiation dose can be witnessed in comparison to levels reached in X-ray computed tomography (CT), which employs an external X-ray source performing a 360° rotation together with the detector to record the body's anatomy (e.g., SPECT effective dose is 2.5 mSv against the 8 mSv of abdominal CT<sup>[33]</sup>).

In this study, Technetium-99m ( $^{99m}\text{Tc}[\text{Tc}]$ ,  $t_{1/2} = 6$  h) was selected for use as the radioisotope as it can easily form  $^{99m}\text{Tc}[\text{Tc}]$ -based compounds. Four different  $^{99m}\text{Tc}[\text{Tc}]$ -based compounds were investigated as contrast agents. Pertechnetate ( $\text{TcO}_4^-$ ;  $^{99}\text{Mo}/^{99m}\text{Tc}$  generator, Mallinckrodt, Petten, The Netherlands), neurotensin-His-tag  $^{99m}\text{Tc}[\text{Tc}]$ -tricarboxyl nuclide (Nuclide)<sup>[34,35]</sup>  $^{99m}\text{Tc}[\text{Tc}]$  colloid (Nanocolloid) and  $^{99m}\text{Tc}[\text{Tc}]$ -Exametazim (d,l-hexamethylpropylenaminoxim) (d,l HMPAO; ROTOP Pharmaka GmbH Dresden Germany) were

employed as imaging agents and included in the PEGDA solution at a 30% v/v concentration, prior to the polymerization process. This concentration was optimal for imaging, and did not compromise the hydrogel polymerization.

The initial stage was to assess the ability of the hydrogel to retain the imaging agent in its matrix. The microrobots were then washed to remove the surface excess of radioactive compound. The spontaneous release in a phosphate buffer solution (PBS) at room temperature was evaluated for 2 h through a gamma counter for 0.5, 1.5, and 3 mm microrobots in the folded configuration. This time interval was considered relevant in relation to clinical procedures. Hydrogel microrobots containing  $\text{TcO}_4^-$  exhibited a release of 90% of the contrast agent in the first 5 min (results not shown), and subsequently a residual radioactivity below the sensitivity of SPECT (that avoided microrobots imaging). In this situation, the release of  $\text{TcO}_4^-$  was expected due to its ionic nature and tendency to diffuse from the hydrogel matrix. Radioactive compound release was lower in the three remaining cases with  $^{99m}\text{Tc}[\text{Tc}]$  nanocolloid giving the optimal inclusion in the microrobot structure, with a residual radioactivity between 80% and 95% on microrobot dimensions (Figure 2B). The residual radioactivity for  $^{99m}\text{Tc}$ -based HMPAO and the nuclide was always below 50% and 28% respectively. Suboptimal inclusion resulted in an unwanted imaging agent release that could hamper microrobot imaging through SPECT. This release could create a radioactivity distribution in areas dissociated from the microrobot itself. A poor retention implies a low residual radioactivity, which results in low quality imaging, especially at smaller dimensions, corresponding to a smaller volume of the doped hydrogel.

Next, the feasibility of performing SPECT imaging of soft microrobots with different dimensions and configuration (folded and unfolded states) was assessed. Image reconstruction and registration among CT and SPECT images confirmed microrobot identification. Both SPECT and CT images were recorded from different cutting planes: coronal, sagittal, and transversal. As expected, hydrogel microrobots doped with HMPAO and Nuclide were not well resolved by SPECT due to a weak retention of the imaging agent by the hydrogel matrix. In these cases, only hydrogels with a size of 3 mm could be identified due to their relatively high volume, incorporating more radioactive compound (Figure 3).

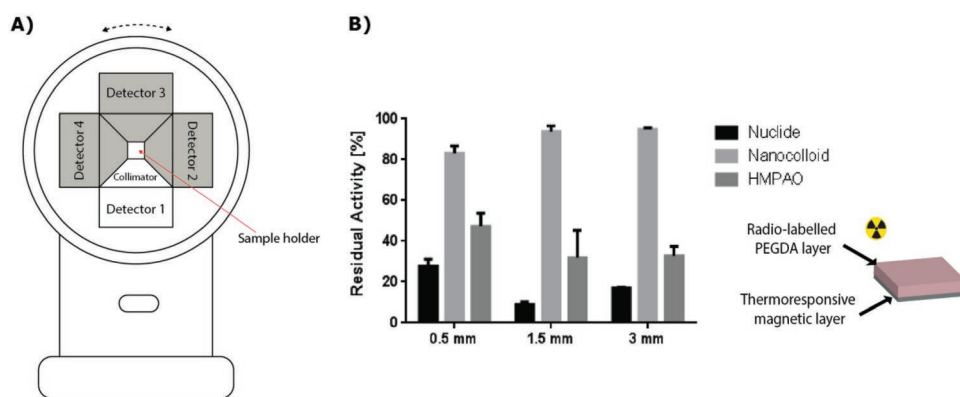


**Figure 2.** A) Schematization of a 4-head multiplexing multi-pinhole camera SPECT system. B) Microrobot residual radioactivity after 2 h of incubation at room temperature for different radioactive compounds and microrobots dimension.

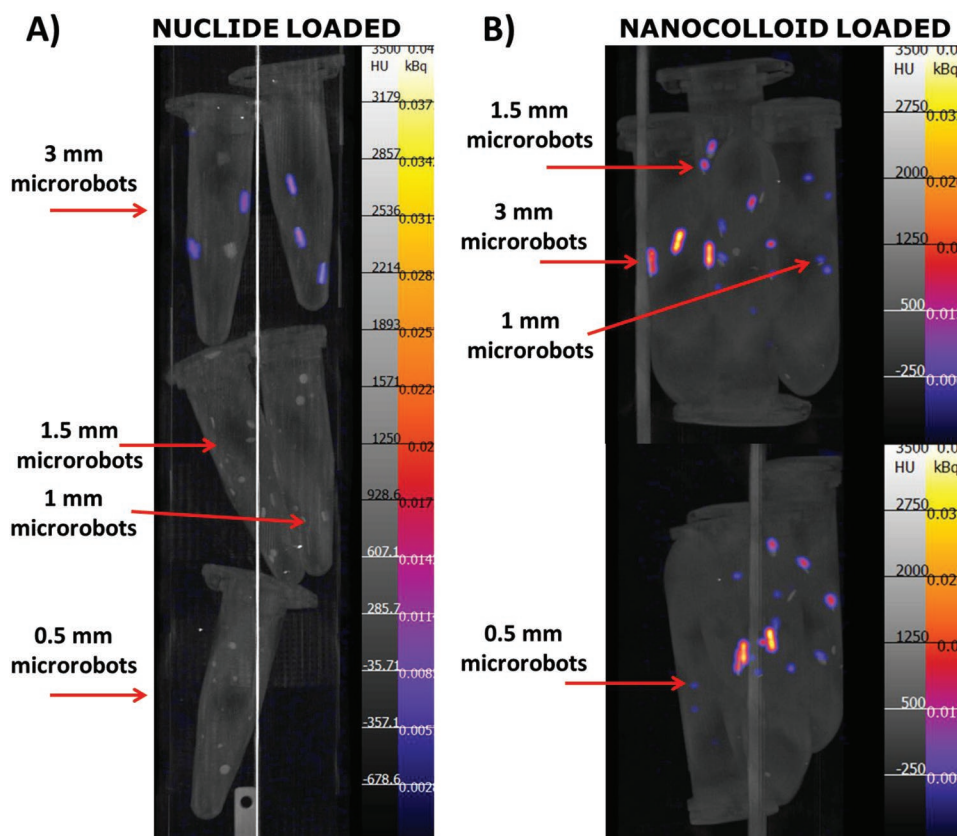


**Figure 3.** SPECT imaging of 3, 1.5, 1, and 0.5 mm microrobots embedding A)  $^{99m}\text{Tc}[\text{Tc}]$ -radionuclide and B)  $^{99m}\text{Tc}$  colloid. In both the images the same color scale has been employed.

However,  $^{99m}\text{Tc}[\text{Tc}]$  colloid-doped microrobots could be resolved using SPECT, for all dimensions (down to 0.5 mm) and in both configurations (folded and unfolded). This was due to a better retention of the colloid nanoparticles by the hydrogel matrix, in comparison to the other radioactive compounds tested. **Figure 4A** (second row) shows that it is possible to image a tubular hydrogel microrobot with a length of 500  $\mu\text{m}$  and a diameter of 100  $\mu\text{m}$ . We also ran CT images for comparison along the same cutting planes (**Figure 4A–D**, first row) to ensure that the radioactivity distribution detected by SPECT corresponded to the microrobots, and not to free or released radionuclide which had been dispersed in the medium. CT imaging was enabled by magnetic nanoparticles inclusion, but is used here only as comparison. We also used SPECT on a 3 mm microrobot to assess the feasibility of detecting a change in the morphological configuration. **Figure 4E** shows that SPECT was able to identify the morphological transformation of the microrobot from the unfolded (planar) to the folded (tubular) configuration. This reinforces the suitability of the proposed clinical imaging technique to monitor soft microrobots and to detect their shape transformation. Shape change could be used as a triggering mechanism for drug release activation and for modulating locomotion performance. Comparison between SPECT and optical microscope images revealed that, in addition of being able to detect shape transformation, SPECT provides accurate microrobots images. Its

ability to represent microrobots shape and features appears comparable to bright field optical microscopy (**Figure S5**, Supporting Information).

After successful imaging of the hydrogel microrobots, we also performed ex vivo imaging. Microrobots with different dimensions and doped with  $^{99m}\text{Tc}[\text{Tc}]$  colloid were injected ex vivo in the intraperitoneal cavity of a mouse. A SPECT acquisition was performed after the implantation, thus showing that microrobots can be clearly detected in the mouse abdomen, both in the sagittal and coronal views.

Although in-body high resolution imaging is undoubtedly crucial for future successful employment of microrobots in clinical practice, this method needs more research. The use of medical imaging strategies for microrobot localization and for verifying the successful performance of a therapeutic function (e.g., shape transition, to enable drug release) would speed up the clinical translation of these miniaturized machines. This study demonstrates that it is possible to load soft shape-switching microrobots with  $^{99m}\text{Tc}[\text{Tc}]$ -based imaging agents and to efficiently view them through SPECT, both in vitro and ex vivo, for different microrobot dimensions and configurations. The study also shows for the first time, that it is possible to perform single microrobot imaging when using hydrogel structures as low as 100  $\mu\text{m}$  in diameter. The results of this report represent a significant step forward for future development in the field of single-robot closed-loop control and activation, leading to

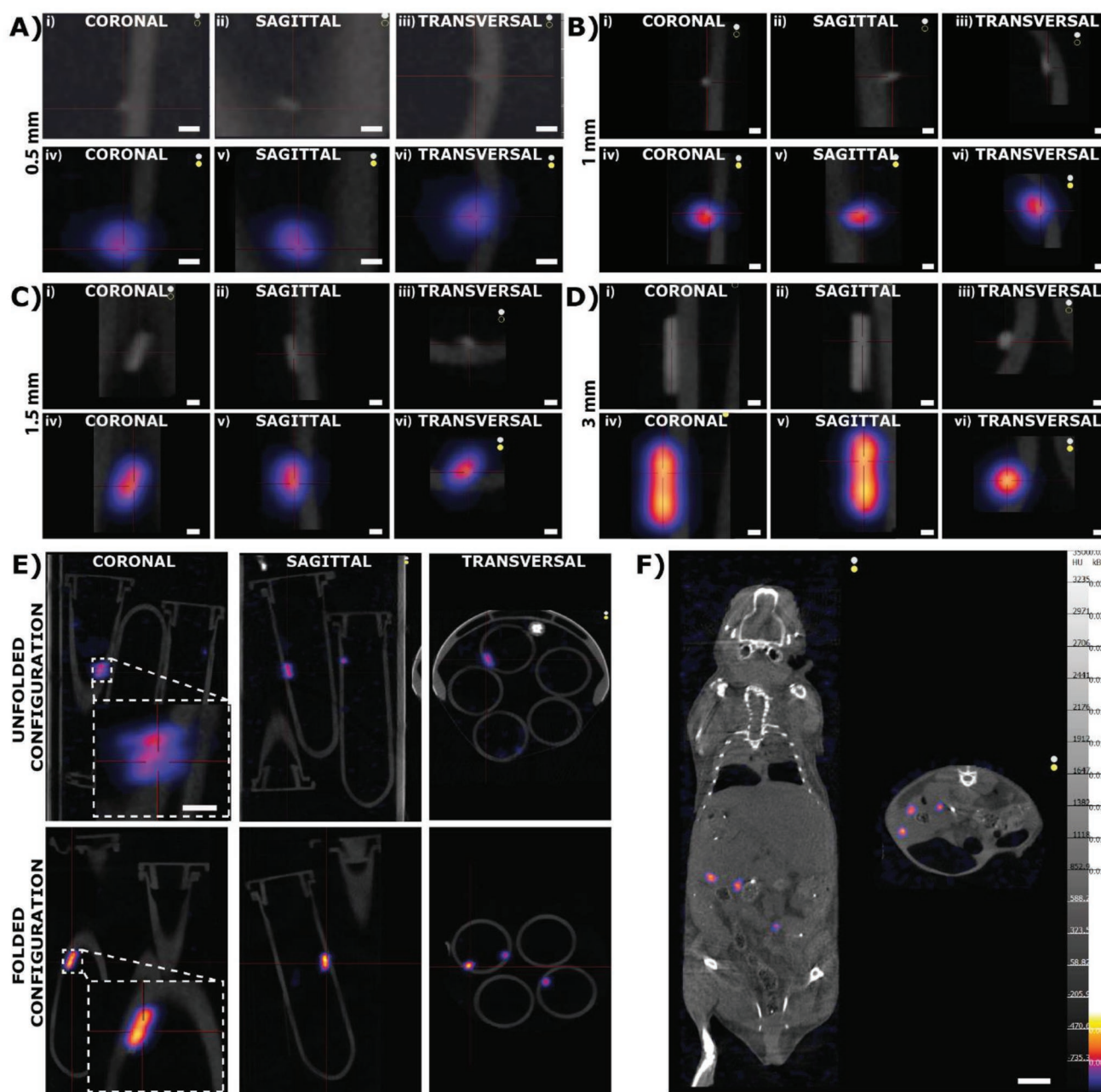


**Figure 4.** CT and SPECT imaging of the theranostic microrobots loaded with  $^{99m}\text{Tc}$  nanocolloid. CT and SPECT imaging of a single A) 0.5 mm, B) 1 mm, C) 1.5 mm, and D) 3 mm microrobot. For each microrobot dimension, projections along the three main cutting planes are reported (scale bar 500  $\mu\text{m}$ ). E) In vitro 3 mm microrobot SPECT images in the folded and unfolded configurations along the three main cutting planes. This result demonstrates the ability to use this imaging technique to track microrobot shape transition (scale bar 2 mm). F) Ex vivo imaging of radiolabeled microrobots subcutaneously injected in mice (test duration about 9 h). Images along the sagittal and coronal cutting plane are reported (scale bar 10 mm).

the innovative and clinically feasible medical application of microrobots.

## Experimental Section

**Microrobots Fabrication:** NIPAAM, AAM, PEGDA (average  $M_w$  575, PEGDA), DMPA (99%) and EL (98%) employed in microrobot fabrication were purchased from Sigma Aldrich. NIPAAM-AAM-PEGDA

(molar ratio 85/15/1) solution, with 3 wt% DMPA photoinitiator and 70 wt% EL, was used for the thermoresponsive layer production. 1 wt% silica-coated  $\gamma\text{-Fe}_2\text{O}_3$  nanoparticles was added and dispersed into the solution by ultrasonication. The amounts of AAM and crosslinking agent (PEGDA) to be embedded in the hydrogel structure were selected to achieve a lower critical solution temperature (LCST) of around 42  $^\circ\text{C}$ , with a suitable swelling ratio.

The microrobots were the result of a two-step, backside exposure, photolithographic process (Figure 1B), where the two different layers were created on a glass photo mask, without alignment. The thickness

of the layers was controlled using an SU-8 spacer which was previously fabricated on silicon wafers using standard photolithography. To prevent adhesion of the hydrogels, a nonadhesive layer was evaporated onto spacer substrates through an overnight silanization process and then activated at 90 °C. Glass masks allowed the microrobots to achieve the desired 2D shape which was obtained by standard photolithography using a positive photoresist (AZ4562). A 100 nm chromium layer was evaporated onto the glass substrates and then removed from the featured areas by rinsing the photoresist with acetone and isopropanol. The two different layers were fabricated in sequence. The first step involved the use of a NIPAAAM-AAM-PEGDA-MNP solution deposition on a silicon substrate provided with SU-8 spacers, with particle alignment under a unidirectional magnetic field, and UV polymerization on the glass mask to obtain monolayer square robots (under a 365 nm UV lamp for 60 s).

After separating the two substrates, the cured NIPAAAM-AAM-PEGDA layer remained attached to the mask side which allowed to proceed with the second step. To add the supporting layer, the PEGDA+RADIOACTIVE COMPOUND/DRUG solution was deposited on a thicker spacer substrate before mask placement. Polymerization was carried out for an additional 90 s under UV light (365 nm). After curing, the bilayers attached to the mask were released through immersion in water.

The same fabrication process was employed to obtain microrobots of different dimensions (in the range 0.5–3 mm of side) by varying the glass mask pattern and the SU-8 spacer thickness (Table S1, Supporting Information). For imaging tests and radioactive compound inclusion, the microrobot fabrication process was carried out according to the established protocol in a glovebox and with an optimized overflow to avoid radioactive contamination.

**Microrobot Imaging:**  $\text{TcO}_4^-$  (pertechnetate) was obtained by  $^{99\text{m}}\text{Tc}[\text{Tc}]$  elution in saline solution. Nuclide solution was obtained by labeling  $^{99\text{m}}\text{Tc}[\text{Tc}]$  in its stable oxidation state, namely  $^{99\text{m}}\text{Tc}$ -tricarbonyl, with Neurotensin by using inverted Histidine (His-tag) as a binding ligand. The binding produced more stable molecules, which allowed a better embedding in the polymeric matrix. A metallic reducing agent, zinc, was used to obtain colloidal pertechnetate dispersion by reducing  $\text{TcO}_4^-$  to a lower oxidation state. Zinc chloride ( $\text{ZnCl}_2$ , Sigma Aldrich) was added to the  $\text{TcO}_4^-$  solution at a concentration of 4 mg mL<sup>-1</sup> to obtain a  $^{99\text{m}}\text{Tc}[\text{Tc}]$  colloid. A  $^{99\text{m}}\text{Tc}$ -Exametazim (d,l-Hexamethyl-propylenaminoxim) kit (ROTOP Pharmaka GmbH), typically employed for SPECT brain imaging, was used to obtain HMPO and to test the behavior of a lipophilic compound. The mouse for ex vivo test was obtained from Paul Scherrer Institute and previously sacrificed for another experiment, therefore no further approval was required.

In all cases, the radioactive compound release was evaluated for 0.5, 1.5, and 3 mm microrobots over 2 h. Microrobots that had previously undergone a washing process aimed at removing the residual radioactive compound were placed on the microrobot external surface and were incubated at room temperature in 1 mL of PBS in order to test the spontaneous release. 20 μL samples were collected from the incubation medium at 5, 15, 30, 60, 90, and 120 min intervals. At the end of the test, the microrobots were collected from the incubation medium in order to measure their residual radioactivity. The radioactivity in all the collected samples was measured using a Gamma counter. The release profiles were not reproducible for all the tested compounds, due to a high inhomogeneity in the incubation solution and to the nonlinear release kinetics (data not shown).

Radioactive microrobots of various dimensions were placed in Eppendorf tubes. CT/SPECT imaging was performed through a CT-Nano SPECT equipped with a 1 mm diameter pinhole aperture (Ref: NSP-108-M14-WB). Image reconstruction and registration among CT and SPECT images, aimed at superimposing the two sets of data to prove microrobot identification (and to distinguish them from accidental radioactive compound droplets), were achieved using the manufacturers HiSPECT software. Image processing and interpretation was performed using the VivoQuant (inviCRO, Boston, MA) software.

## Supporting Information

Supporting Information is available from the Wiley Online Library or from the author.

## Acknowledgements

We acknowledge partial support of this research through the ERC Advanced Grant 743217 – Soft Micro Robotics (SOMBOT). SP acknowledges partial support from the ERC-2017-CoG HINBOTS Grant No. 771565.

## Conflict of Interest

The authors declare no conflict of interest.

## Keywords

drug delivery, imaging, microrobotics, soft microrobots, SPECT

Received: February 7, 2019

Revised: May 7, 2019

Published online: July 15, 2019

- [1] S. Tottori, B. J. Nelson, *Small* **2018**, *14*, 1800722.
- [2] C. Hu, S. Pané, B. J. Nelson, *Annu. Rev. Control, Robot., Auton. Syst.* **2018**, *1*, 53.
- [3] X. Z. Chen, B. Jang, D. Ahmed, C. Hu, C. De Marco, M. Hoop, F. Mushtaq, B. J. Nelson, S. Pané, *Adv. Mater.* **2018**, *30*, 1705061.
- [4] J. Li, B. E.-F. de Ávila, W. Gao, L. Zhang, J. Wang, *Sci. Rob.* **2017**, *2*, eaam6431.
- [5] S. Ornes, *Proc. Natl. Acad. Sci. USA* **2017**, *114*, 12356.
- [6] F. Mou, C. Chen, Q. Zhong, Y. Yin, H. Ma, J. Guan, *ACS Appl. Mater. Interfaces* **2014**, *6*, 9897.
- [7] J. Yu, L. Zhang, *IEEE-ASME Trans. Mech.* **2018**, *24*, 154.
- [8] S. K. Srivastava, G. Clergeaud, T. L. Andresen, A. Boisen, *Adv. Drug Delivery Rev.* **2018**, *138*, 41.
- [9] M. Luo, Y. Feng, T. Wang, J. Guan, *Adv. Funct. Mater.* **2018**, *28*, 1706100.
- [10] V. Iacovacci, G. Lucarini, L. Ricotti, P. Dario, P. E. Dupont, A. Menciassi, *Biomed. Microdevices* **2015**, *17*, 63.
- [11] M. Hoop, A. S. Ribeiro, D. Rösch, P. Weinand, N. Mendes, F. Mushtaq, X. Z. Chen, Y. Shen, C. F. Pujante, J. Puigmartí-Luis, J. Paredes, B. J. Nelson, A. P. Pêgo, S. Pané, *Adv. Funct. Mater.* **2018**, *28*, 1705920.
- [12] B. E.-F. de Ávila, P. Angsantikul, J. Li, M. A. Lopez-Ramirez, D. E. Ramírez-Herrera, S. Thamphiwatana, C. Chen, J. Delezuk, R. Samakapiruk, V. Ramez, *Nat. Commun.* **2017**, *8*, 272.
- [13] J. Li, X. Li, T. Luo, R. Wang, C. Liu, S. Chen, D. Li, J. Yue, S.-h Cheng, D. Sun, *Sci. Rob.* **2018**, *3*, eaat8829.
- [14] X. Wang, X. H. Qin, C. Hu, A. Terzopoulou, X. Z. Chen, T. Y. Huang, K. Maniura-Weber, S. Pané, B. J. Nelson, *Adv. Funct. Mater.* **2018**, *28*, 1804107.
- [15] U. Bozuyuk, O. Yasa, I. C. Yasa, H. Ceylan, S. Kizilel, M. Sitti, *ACS Nano* **2018**, *12*, 9617.
- [16] V. Iacovacci, L. Ricotti, E. Sinibaldi, G. Signore, F. Vistoli, A. Menciassi, *Adv. Sci.* **2018**, *5*, 1800807.
- [17] M. Medina-Sánchez, O. G. Schmidt, *Nature* **2017**, *545*, 406.

- [18] B. Wang, Y. Zhang, L. Zhang, *Quant. Imaging Med. Surg.* **2018**, *8*, 461.
- [19] S. Pané, J. Puigmartí-Luis, C. Bergeles, X. Z. Chen, E. Pellicer, J. Sort, V. Počepcová, A. Ferreira, B. J. Nelson, *Adv. Mater. Technol.* **2019**, *4*, 1800575.
- [20] A. Servant, F. Qiu, M. Mazza, K. Kostarelos, B. J. Nelson, *Adv. Mater.* **2015**, *27*, 2981.
- [21] D. Vilela, U. Cossío, J. Parmar, A. M. Martínez-Villacorta, V. Gómez-Vallejo, J. Llop, S. Sanchez, *ACS Nano* **2018**, *12*, 1220.
- [22] K. Cha, S. Jeong, J. Choi, L. Qin, J. Li, J. Park, S. Park, presented at *Annual Int. Conf. IEEE Engineering in Medicine and Biology*, Buenos Aires, Argentina, August **2010**.
- [23] I. S. Khalil, P. Ferreira, R. Eleutério, C. L. de Korte, S. Misra, *IEEE Int. Conf. Rob. Autom.* **2014**, *8*, 3807.
- [24] P. Pouponneau, G. Soulez, G. Beaudoin, J.-C. Leroux, S. Martel, *Cardiovasc. Inter. Rad.* **2014**, *37*, 784.
- [25] X. Yan, Q. Zhou, M. Vincent, Y. Deng, J. Yu, J. Xu, T. Xu, T. Tang, L. Bian, Y.-X. J. Wang, *Sci. Rob.* **2017**, *2*, eaaq1155.
- [26] N. A. Peppas, J. Z. Hilt, A. Khademhosseini, R. Langer, *Adv. Mater.* **2006**, *18*, 1345.
- [27] D. a. Trel'ová, A. R. Salgarella, L. Ricotti, G. Giudetti, A. Cutrone, P. Šrámková, A. Zahoranova, D. a. Chorvát Jr, D. Hasko, C. Canale, S. Micera, J. Kronek, A. Menciassi, I. Lacič, *Langmuir* **2018**, *35*, 1085.
- [28] S. Palagi, P. Fischer, *Nat. Rev. Mater.* **2018**, *3*, 113.
- [29] G. Liang, Z. Yang, R. Zhang, L. Li, Y. Fan, Y. Kuang, Y. Gao, T. Wang, W. W. Lu, B. Xu, *Langmuir* **2009**, *25*, 8419.
- [30] H.-W. Huang, M. S. Sakar, A. J. Petruska, S. Pané, B. J. Nelson, *Nat. Commun.* **2016**, *7*, 12263.
- [31] S. Fusco, M. S. Sakar, S. Kennedy, C. Peters, R. Bottani, F. Starsich, A. Mao, G. A. Sotiriou, S. Pané, S. E. Pratsinis, D. Mooney, B. J. Nelson, *Adv. Mater.* **2014**, *26*, 952.
- [32] K. Malachowski, J. Breger, H. R. Kwag, M. O. Wang, J. P. Fisher, F. M. Selaru, D. H. Gracias, *Angew. Chem.* **2014**, *126*, 8183.
- [33] F.D.A. Radiation emitting products, <https://www.fda.gov/radiation-emitting-products/medical-x-ray-imaging/what-are-radiation-risks-ct>, (accessed: June 2019).
- [34] A. Badar, J. Williams, R. T. de Rosales, R. Tavaré, F. Kampmeier, P. J. Blower, G. E. Mullen, *EJNMMI Res.* **2014**, *4*, 14.
- [35] A. Egli, R. Alberto, L. Tannahill, R. Schibli, U. Abram, A. Schaffland, R. Waibel, D. Tourwé, L. Jeannin, K. Iterbeke, *J. Nucl. Med.* **1999**, *40*, 1913.